Effect of crosslinking in cartilage-like collagen microstructures

Ying-chun Chen[a], Minsi Chen[b], Eamonn A Gaffney[c], Cameron P Brown[a,*]

[a] *Botnar Research Centre, NDORMS, University of Oxford, UK*
[b] *Department of Computing and Mathematics, University of Derby, UK*
[c] *Wolfson Centre for Mathematical Biology, Mathematical Institute, University of Oxford, UK*

Abstract

The mechanical performance of biological tissues is underpinned by a complex and finely balanced structure. Central to this is collagen, the most abundant protein in our bodies, which plays a dominant role in the functioning of tissues, and also in disease. Based on the collagen meshwork of articular cartilage, we have developed a bottom-up spring-node model of collagen and examined the effect of fibril connectivity, implemented by crosslinking, on mechanical behaviour. Although changing individual crosslink stiffness within an order of magnitude had no significant effect on modelling predictions, the density of crosslinks in a meshwork had a substantial impact on its behaviour. Highly crosslinked meshworks maintained a 'normal' configuration under loading, with stronger resistance to deformation and improved recovery relative to sparsely crosslinked meshwork. Stress on individual fibrils, however, was higher in highly crosslinked meshworks. Meshworks with low numbers of crosslinks reconfigured to disease-like states upon deformation and recovery. The importance of collagen interconnectivity may provide insight into the role of ultrastructure and its mechanics in the initiation, and early stages, of diseases such as osteoarthritis.

Keywords: articular cartilage, cartilage model, osteoarthritis, ultrastructure, collagen network model

1. Introduction

Articular cartilage performs an impressive mechanical function, which is underpinned by a hierarchical structural configuration of type II collagen, proteoglycans, and interstitial fluid [1]. As one of the main determinants of function in the tissue, changes to the collagen meshwork are central to disease processes [2, 3, 4, 5]. Collagen-collagen interactions dominate the cohesive strength of the matrix [6] and therefore the resistance to mechanical damage progression.

The breakdown from the intermeshed, pseudo-random collagen configuration at the micrometer scale to form aligned fibre bundles has been identified as a mechanically irreversible

*Correspondence
Email address: cameron.brown@ndorms.ox.ac.uk (Cameron P Brown)

step in the damage process [4] and has long been associated with abnormal cartilage softening [7]. A recent study has further found localised regions of collagen meshwork disruption and reconfiguration at early stages of disease before the appearance of histological changes [8]. An improved understanding of the mechanics of the collagen meshwork, and the implications of its properties and connectivity, is therefore of interest for osteoarthritis pathogenesis, diagnostics and the design of regenerative medicine strategies.

Computational modelling provides an ideal platform from which to explore mechano-structural changes. In recent years, increasingly sophisticated constitutive models have been developed to represent tissue-level cartilage mechanics [9, 10, 11, 12, 13, 14]. With this sophistication has come an improved representation of structure. Wilson et al., for example, integrated the relation between permeability and tissue composition with a viscoelastic constitutive relation within a fibril-reinforced model for predicting the equilibrium and transient response of articular cartilage during compression, indentation and swelling tests [9]. Ateshian et al. applied continuous fibre angular distributions to model the solid matrix of cartilage and successfully predicted experimental observations of the tissue's equilibrium response to mechanical and osmotic loading [11].

However, such models do not incorporate details from individual fibres but instead consider the impact of average fibril orientations on the scale of continuum. In particular, while there have been advances in the theoretical mechanics of upscaling (e.g.[15, 16, 17]), whereby material properties at the sub-continuum scale are systematically incorporated into the constitutive relation of continuum models with controlled accuracy, such approaches are generally not tractable for collagen networks and cartilage [18, 19]. Hence, it is currently not feasible to assess the impact of fibril-scale changes and individual crosslinks in a continuum model. Thus one must instead adopt a bottom-up approach and represent collagen fibrils individually; furthermore elastic dominated constitutive relationships are indicated for fibrils [18] in contrast to entropic dominated models at lower scales. An exemplar of such a model has already been explored by Lee et al [20], who concentrate on elucidating the stress strain relationship of material made from networks of collagen fibrils. In contrast, here, our objective is to explore how crosslink properties and densities within a collagen meshwork representing cartilage impact on mechanical performance and structure, in particular fibril alignment as it is a signature of cartilage pathology [7, 21, 4].

2. Methods

2.1. Collagen structure simulation

A 2-D model of collagen structure was implemented in C/C++. For simplicity collagen fibrils were not represented as Euler-Bernoulli filaments; instead each fibril was modelled as a series of 1-D springs of length approximately 1 μm connected at nodes, via torque free pin joints. Assuming a fibril diameter of 100 nm and a linear stress-strain relation, the material property of the fibrils were calculated by fitting experimental data from a single fibril tensile test [22] to give a force-strain relation of 4 μN/unit strain (equivalent to a Young's modulus $\approx$ 500 MPa). Crosslinks were implemented with a linear force-strain relation on the assumption of small deformation, with parameters chosen a posteriori due

to a lack of available data. It should be noted that crosslinking in this model refers to inter-fibril connectivity, and does not probe, for example, enzymatic or AGE-related crosslinking [18, 23]. Validation of the fibril implementation was performed using a single fibril of length 20 μm (20 segments) under load in one dimension. Validation of crosslink behaviour was similarly performed by linking two fibrils in series. Each spring had the linear force-strain relation

$$F = k(\frac{L'-L_0}{L_0}), \tag{1}$$

where L' was the displaced length of the spring, L_0 was the resting length of the spring, F was force and k is the spring constant, a material property. The error in the numerical solution, relative to the analytical solution, was considered by calculating the spring length on reaching equilibrium (ie. all spring movement was below a very small tolerance). The accuracy of numerical solution was better than 99.9% (see Table 1).

Table 1: Numerical spring length error under one dimensional tensile test load for an isolated spring segment (single spring) and a single, 20-segment spring (single fibril).

	single spring	single fibril		
Spring resting length	1μm	0.5μm	1μm	2μm
Error(%)	-0.006	-0.022	-0.003	-0.003

Thirty collagen meshwork configurations were constructed to simulate the pseudo-random collagen microstructure observed in electron micrographs [24, 5, 25], with anisotropy and connectivity forming the Benninghoff arcades [26] at larger scales. A representative structure is given in Figure 1A. Each node, shown in yellow, is connected to two neighbours on the same fibre by linear springs, shown in green. All structures were based on 30 parallel sets of 24 springs, giving a total length 24 μm, initially aligned with the y-axis and separated by 1 μm in the x direction. Nodes were then randomly displaced in x direction within $\pm$ 1 μm. Crosslinks (shown in red in Figure 1) were incorporated based on proximity of nodes from adjacent fibrils. Proximity thresholds of 0.3 μm, 0.5 μm and 0.8 μm were applied to each structure, with a linear stress-strain relation for the crosslink varied between 2 and 12 μN/unit strain. Once a crosslink formed in the model, it was not allowed to break.

Uniaxial tensile loading, in the direction of predominant fibril alignment, was applied as an exemplar to simplify the complex stress environment of the tissue while capturing the tensile response of the collagen meshwork to macroscale applied loads [27, 28]. In each simulation, the end nodes of each fibril were fixed in the x-direction and subjected to a constant tensile force of 0.5 μN in the y-direction. Node positions were timestepped according to a linear overdamping law. When the structure reached equilibrium, the load was released and the structure allowed to recover. Node positions were recorded at original, equilibrium and recovered positions and passed to MATLAB (2015a, The MathWorks Inc., Natick, USA) for analysis.

Strains and fibril organisations were calculated for each simulation. Fibril strains in each structure were calculated based on the change in distance between adjacent nodes.

Bulk strains were calculated based on the mean distance between the fibril end nodes. Organisation was classified using an anisotropy parameter r_{mean} based on polarised optical parameters used for cartilage measurements [29, 30, 31], providing a means for comparison with experiments. In particular r_{mean} is defined by

$$r_{mean} = \frac{1}{N} \sum_{i=1}^{N} \frac{\delta Y_i - \delta X_i}{\delta Y_i + 2\delta X_i}, \tag{2}$$

where N is total number of springs, $\delta X_i = |\delta x_{i+1} - \delta x_i|$, $\delta Y_i = |\delta y_{i+1} - \delta y_i|$ and δx_i and δy_i are the x and y positions of the i^{th} node. Note for instance that when $r_{mean} = 1$, the fibrils are aligned in the direction of loading.

3. Results

3.1. Effect of crosslink density

Representative microstructures before and after stretching (along the y direction) and after relaxation are shown in Figure 1. Qualitatively, different numbers of crosslinks resulted in substantially different configurations after loading. Highly-crosslinked microstructures maintained a 'normal' configuration with loading (Figure 2A). Microstructures with lower crosslink densities were more aligned with the direction of loading, and formed fibre bundles (Figure 2B) similar to those observed in electron microscopy of osteoarthritic cartilage (Figure 2C [21]).

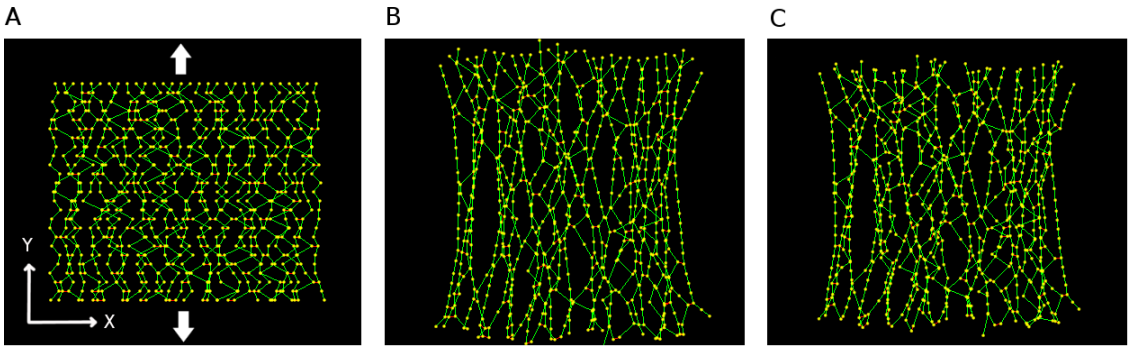

Figure 1: Representative structure before stretching (A), after stretching (B) and after relaxation (C). White arrows show the force direction. Springs shown in green, nodes in yellow and crosslinks in red.

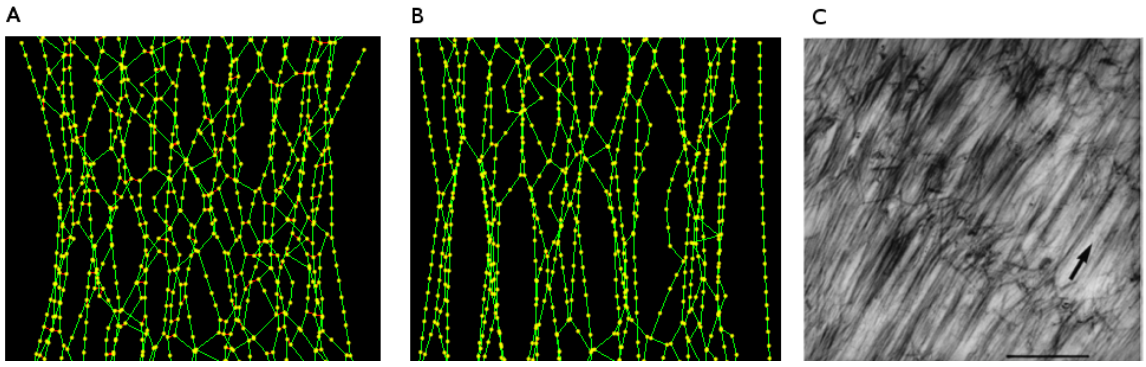

Figure 2: Representative structure with 314 crosslinks (A) and with 81 crosslinks (B) after stretching. Transmission electron micrograph of collagen fibril organisation in osteoarthritic cartilage (C), reproduced from [21]. Scale bar 1.5μm.

For a given structure and crosslinking threshold, the crosslink density was inversely proportional to the anisotropy measure of the pre-loaded meshwork structure (Figure 3), with $r^2 > 0.9$ (Pearson's correlation coefficient).

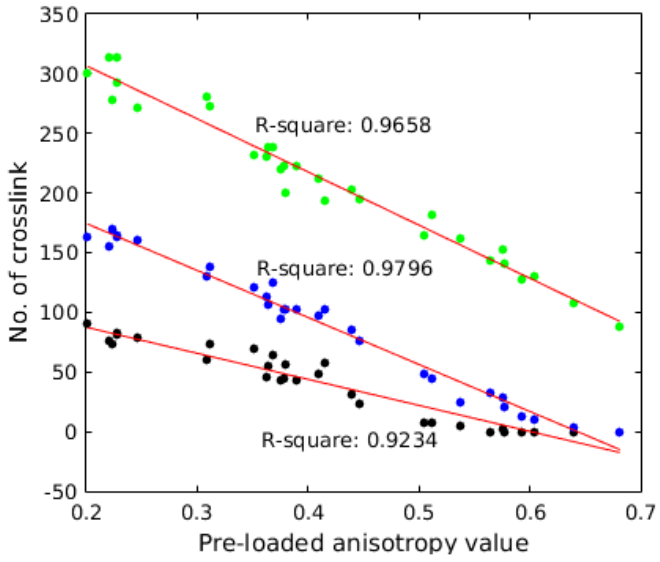

Figure 3: Relationship between crosslink density and angular anisotropy (r_{mean}) of the pre-loaded structure. Each line represents data from a single crosslink threshold. Black represents 0.3 μm, blue represents 0.5 μm and green represents 0.8 μm crosslink proximity thresholds.

Quantitative differences due to crosslink density were also observed. Due to the random modification of node positions for each microstructure, threshold distances for crosslinking

produced a range of crosslink densities in the structures. The reconfiguration of fibrils under loading, quantified by the above anisotropy parameter r_{mean} (equation 2) is presented in Figure 4. At low crosslink densities, fibrils aligned with the direction of load, with minimal recovery. At higher crosslink densities, the microstructures resisted realignment (Figure 4A) and recovered their isotropy to a greater extent (Figure 4C). The maximum recovery of isotropy (% recovered r_{mean} relative to r_{mean} at equilibrium), however, was only 35%.

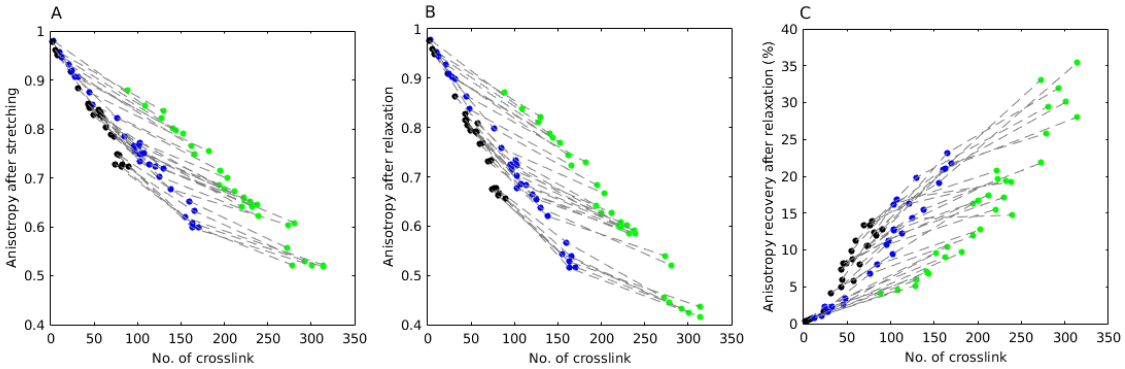

Figure 4: Structural anisotropy as defined by r_{mean} under loading and recovery. Greater isotropy was maintained (A), and recovered (B,C), in highly crosslinked microstructures. Dashed lines plot the trends within the same structure at different crosslink thresholds. Different crosslink proximity thresholds are presented with colours where 0.3 μm is shown in black, 0.5 μm is shown in blue and 0.8 μm is shown in green.

For a fixed crosslink proximity threshold, bulk strain data clustered into groups. Within these groups (i.e. black, green or blue dots in Figure 5), bulk strain increased with increasing crosslink density, both after stretching (Figure 5A) and after relaxation (Figure 5B). This was likely due to the relationship between crosslink density and angular isotropy in the pre-loaded state (Figure 3), and therefore greater structural reconfiguration under load. Within a structural configuration (linked by dashed lines, Figure 5), however, increasing crosslink densities consistently reduced bulk strain. In both cases, greater bulk strain was recovered upon relaxation with increasing crosslink density (Figure 5C).

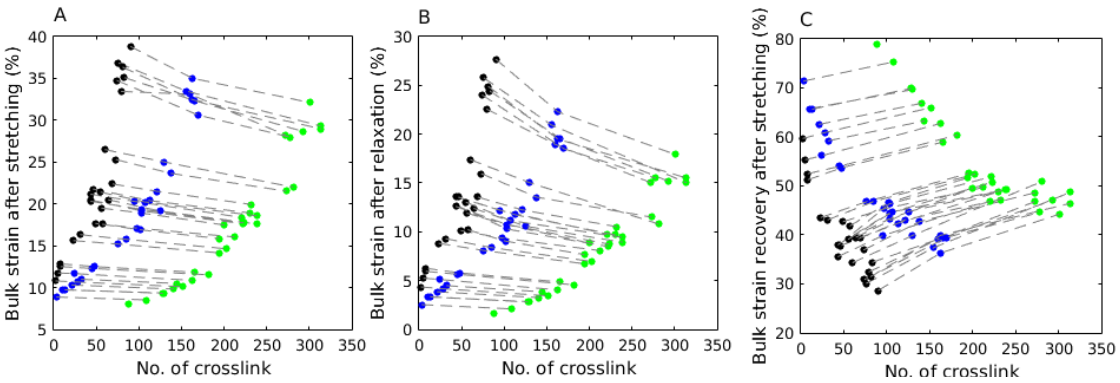

Figure 5: Bulk mechanical strain under loading and recovery. Bulk strain decreased with increasing crosslink density (A,B), with greater recovery in highly crosslinked microstructures (C). Dashed lines plot the trends within the same structure at different crosslink proximity thresholds. Different crosslink proximity thresholds are presented with colours where 0.3 μm is shown in black, 0.5 μm is shown in blue and 0.8 μm is shown in green.

Fibril strain (the mean of the distribution of fibril strains) after stretching increased with crosslink density (Figure 6). Two exceptions to this trend were apparent, however, reasons for this are unclear. Recovery of fibril strain after relaxation was near 100%, with mean fibril strain reduced to $0.037 \pm 0.004\%$.

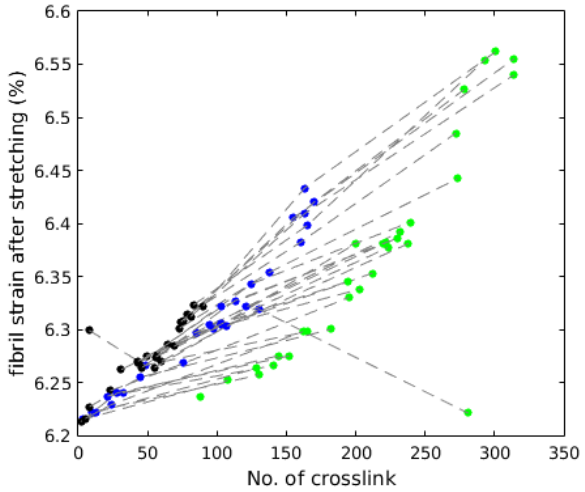

Figure 6: Fibril strain at equilibrium at different crosslink densities. Dashed lines link the same structure with different crosslink threshold. Different crosslink threshold shows in different colour where 0.3 μm is shown in black, 0.5 μm is shown in blue and 0.8 μm is shown in green.

3.2. Effect of crosslink stiffness

Six different material properties were assigned to test the effects of crosslink properties on the mechanical behaviour of the microstructure. Output parameters generated for a

representative structure are given in Table 2. Kruskal-Wallis tests (SPSS Statistics 17.0, IBM) showed no significant differences (all $p > 0.4$) in the structural response to loading for different crosslink stiffnesses.

Table 2: Mechanical behaviour of a representative structure (293 crosslinks) with different crosslink stiffness.

Output parameter	Material property of crosslink (Force (μN)/unit strain)					
	2	4	6	8	10	12
fibril strain at equilibrium (%)	6.540	6.554	6.560	6.563	6.565	6.566
bulk strain at equilibrium (%)	28.935	28.654	28.549	28.493	28.459	28.435
anisotropy at equilibrium	0.439	0.433	0.431	0.430	0.429	0.429
fibril strain after relaxation (%)	0.037	0.036	0.036	0.036	0.035	0.035
bulk strain after relaxation (%)	17.306	17.296	17.289	17.283	17.279	17.276
anisotropy after relaxation	0.362	0.362	0.362	0.362	0.362	0.362

4. Discussion

Using a bottom-up model of a cartilage-like collagen meshwork, we have demonstrated the effect of fibril interconnectivity, represented by crosslinking, on restructuring under load. Although crosslink stiffness, within the parameter range considered, had no significant effect, the number of crosslinks in each structure consistently altered the structural response to loading, in agreement with previously published studies, though these are based on entropy-based mechanics [32] in contrast to the elastic dominated regime adopted here for collagen fibrils [18]. Increasing crosslink density increased resistance to bulk deformation, and improved the recovery of both bulk deformation (Figure 5) and structural isotropy (Figure 4). This improved resistance to network reconfiguration under loading, though at the expense of higher stresses for the collagen fibrils themselves (Figure 6).

In the context of cartilage and cartilage degradation, this may provide an insight into the mechanisms underpinning the transition from a normal, intact meshwork to the degraded collagen architecture observed in experimental studies [24]. In particular, a highly connected meshwork was predicted to maintain its 'normal' configuration under loading. In Figure 2A for example, the highly crosslinked structure maintained its pseudorandom organisation after loading, also shown by the lower anisotropy at high crosslink densities in Figure 4. The same structures with lower connectivity, however, transformed to a 'diseased' configuration (Figure 2B). This 'diseased' configuration, as observed experimentally by electron microscopy (e.g. [21], Figure 2C) of osteoarthritic cartilage, was characterised by bundling of fibrils in the direction of applied force, and increased anisotropy (Figure 4).

Expanding findings and hypotheses from previous experimentally-driven studies [4, 8, 25] which focussed on structural disease progression rather than initiation, the role of collagen connectivity provides insight into the mechanisms by which bundle formation and micro cracking occur. Small regions of fibril alignment, of the size of a few tens of microns for example, have been observed in the deep zone of human cartilage sections prior to changes

in histological score, with increasing bundling during progression [8]. While progression can be explained by stress concentrations and critical-size crack formation, the initiation of bundling may be explained by a local loss of connectivity through the breaking/removal of crosslinks with the latter being consistent with the modelling predictions presented here. Specifically, high inter-fibril connectivity appears critical in maintaining the balance between swelling pressure and collagen tension [33] required for cartilage function.

In this context, the same effect would be obtained by either a loss of direct collagen-collagen connectivity or the loss of physical separation of fibrils by aggrecan digestion. Our results suggest, due to the increased stress on a fibril level in highly crosslinked structures (Figure 6), that such restructuring is likely to be driven by damage to connecting elements rather than the collagen fibrils themselves. The reduced fibril-level strain observed with reduced connectivity further suggests that recovery from a 'diseased' collagen configuration is energetically unfavourable while loading is maintained. In addition to describing disease processes, this model may be expanded to provide an additional platform for the design of fibre-based scaffolds for tissue engineering, particularly allowing the modification of collagen organisation and properties across tissue interfaces or inter-zonal reconfigurations to recreate physiological cell environments.

The structural realism of our model is limited by two main factors. Firstly, aggrecan, a major component of the cartilage matrix, has not been considered directly. Large aggrecan macromolecules are trapped by, and swell against, the collagen meshwork and play an important role in load carriage. A number of methods have been developed for simulating osmotic pressure in cartilage [34, 35, 36, 37, 38], however, collagen-aggrecan interaction is problematic in a 2-D implementation due to the difficulty in replicating entrapment processes. The generalisation of our model to three dimensions to allow the investigation of these processes is planned for future work, further enabling the resolution of structural response to the complex mechanical environment of the tissue. Secondly, collagen fibril properties have been based on a linear elastic fit to a highly nonlinear material without including viscoelasticity and the related transient response. This transient response, along with the incorporation of material level damage feedbacks, will be necessary for mechanistic insight into the coupling between damage initiation and progression.

5. Conclusion

In this study, we used a node-spring model to investigate the role of inter-fibril connectivity in the cartilage collagen meshwork. The level of interconnectivity (implemented as crosslink density) had a substantial effect on mechanical behaviour of the structure; however, no effect was observed with changes to crosslink stiffness within the regimes considered. Highly crosslinked structures can maintain their configurations under loading more than less-crosslinked structures, and more strongly recover with relaxation after removal of the load, though exhibit a higher level of stress per fibril during bulk deformation. The configurations of less-crosslinked structures were also qualitatively similar to diseased collagen configurations observed in experimental studies. Specifically these structures were more prone to the formation of fibre bundles aligned with the direction of tensile force during a loading and

unloading cycle. This model aids the understanding of the role of collagen structure and mechanics in the initiation of diseases such as osteoarthritis, and may contribute to scaffold design aimed at restoring function in regenerative treatments.

6. Acknowledgement

We gratefully acknowledge financial support from Orthopaedic Research UK (ref 504), the Taiwan Government Scholarship to Study Abroad (GSSA), Arthritis Research UK (grant 20299 and Oxford EOTC), Marie Curie IRSES *skelGEN*, and the Oxford NIHR BRU in musculoskeletal disease.

References

[1] M. Huber, S. Trattnig, F. Lintner, Anatomy, biochemistry, and physiology of articular cartilage, Invest Radiol 35 (10) (2000) 573–580.

[2] W. S. Hwang, B. Li, L. H. Jin, K. Ngo, N. S. Schachar, G. N. Hughes, Collagen fibril structure of normal, aging, and osteoarthritic cartilage, J Pathol 167 (4) (1992) 425–33.

[3] E. B. Hunziker, Articular cartilage repair: are the intrinsic biological constraints undermining this process insuperable?, Osteoarthritis Cartilage 7 (1) (1999) 15–28.

[4] C. P. Brown, M. A. Houle, M. Chen, A. J. Price, F. Legare, H. S. Gill, Damage initiation and progression in the cartilage surface probed by nonlinear optical microscopy, J Mech Behav Biomed Mater 5 (1) (2012) 62–70.

[5] M. Stolz, R. Gottardi, R. Raiteri, S. Miot, I. Martin, R. Imer, U. Staufer, A. Raducanu, M. Duggelin, W. Baschong, A. U. Daniels, N. F. Friederich, A. Aszodi, U. Aebi, Early detection of aging cartilage and osteoarthritis in mice and patient samples using atomic force microscopy, Nat Nanotechnol 4 (3) (2009) 186–192.

[6] N. D. Broom, H. Silyn-Roberts, Collagen-collagen versus collagen-proteoglycan interactions in the determination of cartilage strength, Arthritis Rheum 33 (10) (1990) 1512–7.

[7] N. D. Broom, Abnormal softening in articular cartilage. Its relationship to the collagen framework, Arthritis & Rheumatism 25 (10) (1982) 1209–1216.

[8] C. P. Brown, M. Houle, K. Popov, M. Nicklaus, C. Couture, M. Laliberté, T. Brabec, A. Ruediger, A. J. Carr, A.J.and Price, H. S. Gill, L. Ramunno, F. Légaré, Imaging and modeling collagen architecture from the nano to micro scale, Biomedical Optics Express 5 (2014) 233–43.

[9] W. Wilson, J. M. Huyghe, C. C. van Donkelaar, A composition-based cartilage model for the assessment of compositional changes during cartilage damage and adaptation, Osteoarthritis Cartilage 14 (6) (2006) 554–560.

[10] D. M. Pierce, T. Ricken, G. A. Holzapfel, A hyperelastic biphasic fibre-reinforced model of articular cartilage considering distributed collagen fibre orientations: continuum basis, computational aspects and applications, Comput Methods Biomech Biomed Engin 16 (12) (2013) 1344–1361.

[11] G. A. Ateshian, V. Rajan, N. O. Chahine, C. E. Canal, C. T. Hung, Modeling the matrix of articular cartilage using a continuous fiber angular distribution predicts many observed phenomena, J Biomech Eng 131 (6) (2009) 061003.

[12] W. Wilson, C. C. van Donkelaar, B. van Rietbergen, R. Huiskes, A fibril-reinforced poroviscoelastic swelling model for articular cartilage, J Biomech 38 (6) (2005) 1195–1204.

[13] J. M. Deneweth, S. G. McLean, E. M. Arruda, Evaluation of hyperelastic models for the non-linear and non-uniformhigh strain-rate mechanics of tibial cartilage, J Biomech 46 (10) (2013) 1604–10.

[14] W. Wilson, J. M. Huyghe, C. C. van Donkelaar, Depth-dependent compressive equilibrium properties of articular cartilage explained by its composition, Biomech Model Mechanobiol 6 (1-2) (2007) 43–53.

[15] M. Quintard, S. Whitaker, Transport in ordered and disordered porous media i: The cellular average and the use of weighting functions, Transport in Porous Media 14 (2) (1994) 163–177.

[16] J. H. Cushman, L. S. Bennethum, B. X. Hu, A primer on upscaling tools for porous media, Advances in Water Resources 25 (8) (2002) 1043–1067.
[17] Y. Davit, C. G. Bell, H. M. Byrne, L. A. Chapman, L. S. Kimpton, G. E. Lang, K. H. Leonard, J. M. Oliver, N. C. Pearson, R. J. Shipley, et al., Homogenization via formal multiscale asymptotics and volume averaging: How do the two techniques compare?, Advances in Water Resources 62 (2013) 178–206.
[18] M. J. Buehler, Nature designs tough collagen: explaining the nanostructure of collagen fibrils, Proceedings of the National Academy of Sciences 103 (33) (2006) 12285–12290.
[19] V. Klika, E. A. Gaffney, Y.-C. Chen, C. P. Brown, An overview of multiphase cartilage mechanical modelling and its role in understanding function and pathology, Journal of the Mechanical Behavior of Biomedical Materials 62 (2016) 139 – 157.
[20] B. Lee, X. Zhou, K. Riching, K. W. Eliceiri, P. J. Keely, S. A. Guelcher, A. M. Weaver, Y. Jiang, A three-dimensional computational model of collagen network mechanics, PloS one 9 (11) (2014) e111896.
[21] M. H. Chen, N. Broom, On the ultrastructure of softened cartilage: a possible model for structural transformation, Journal of anatom 192 (Pt 3) (1998) 329–41.
[22] J. A. van der Rijt, K. O. van der Werf, P. J. Bennink, M. L. andDijkstra, J. Feijen, Micromechanical testing of individual collagen fibrils, Macromol Biosci 6 (9) (2006) 697–702.
[23] A. C. Chen, M. M. Temple, D. M. Ng, N. Verzijl, J. DeGroot, J. M. TeKoppele, R. L. Sah, Induction of advanced glycation end products and alterations of the tensile properties of articular cartilage, Arthritis and Rheumatism 46 (12) (2002) 3212–3217. doi:10.1002/art.10627.
URL http://dx.doi.org/10.1002/art.10627
[24] R. Teshima, T. Otsuka, N. Takasu, N. Yamagata, K. Yamamoto, Structure of the most superficial layer of articular cartilage, Journal of Bone & Joint Surgery, British Volume 77-B (3) (1995) 460–464.
[25] N. Broom, M. H. Chen, A. Hardy, A degeneration-based hypothesis for interpreting fibrillar changes in the osteoarthritic cartilage matrix, Journal of anatomy 199 (6) (2001) 683–698.
[26] A. Benninghoff, Form und bau der Gelenknorpel in ihren Bezeihungen zur Funktion, Forschung 2 (2) (1925) 783–825.
[27] W. Wilson, C. van Donkelaar, B. van Rietbergen, K. Ito, R. Huiskes, Stresses in the local collagen network of articular cartilage: a poroviscoelastic fibril-reinforced finite element study, Journal of Biomechanics 37 (3) (2004) 357 – 366. doi:http://dx.doi.org/10.1016/S0021-9290(03)00267-7.
URL http://www.sciencedirect.com/science/article/pii/S0021929003002677
[28] A. Thambyah, N. Broom, Micro-anatomical response of cartilage-on-bone to compression: mechanisms of deformation within and beyond the directly loaded matrix, Journal of Anatomy 209 (5) (2006) 611–622. doi:10.1111/j.1469-7580.2006.00646.x.
URL http://dx.doi.org/10.1111/j.1469-7580.2006.00646.x
[29] M.-A. Houle, C.-A. Couture, S. Bancelin, J. Kolk, E. Auger, C. Brown, K. Popov, L. Ramunno, F. Légaré, Analysis of forward and backward second harmonic generation images to probe the nanoscale structure of collagen within bone and cartilage, Journal of biophotonics 8 (11-12) (2015) 993–1001.
[30] C.-A. Couture, S. Bancelin, J. Van der Kolk, K. Popov, M. Rivard, K. Légaré, G. Martel, H. Richard, C. Brown, S. Laverty, et al., The impact of collagen fibril polarity on second harmonic generation microscopy, Biophysical journal 109 (12) (2015) 2501–2510.
[31] P. J. Campagnola, L. M. Loew, Second-harmonic imaging microscopy for visualizing biomolecular arrays in cells, tissues and organisms, Nat Biotech 21 (11) (2003) 1356–1360.
[32] Y. Jin, T. Wang, Three-dimensional numerical modeling of the damage mechanism of amorphous polymer network, Computational Materials Science 46 (3) (2009) 632 – 638.
[33] A. Maroudas, Balance between swelling pressure and collagen tension in normal and degenerate cartilage, Nature 260 (1976) 808–809.
[34] M. Bathe, G. C. Rutledge, A. J. Grodzinsky, B. Tidor, Osmotic pressure of aqueous chondroitin sulfate solution: a molecular modeling investigation, Biophys J 89 (4) (2005) 2357–71.
[35] W. M. Lai, J. S. Hou, V. C. Mow, A triphasic theory for the swelling and deformation behaviors ofarticular cartilage, J Biomech Eng 113 (3) (1991) 245–258.

[36] P. J. Basser, R. Schneiderman, R. A. Bank, E. Wachtel, A. Maroudas, Mechanical properties of the collagen network in human articular cartilage as measured by osmotic stress technique, Arch Biochem Biophys 351 (2) (1998) 207–19.
[37] E. H. Han, S. S. Chen, S. M. Klisch, R. L. Sah, Contribution of proteoglycan osmotic swelling pressure to the compressive properties of articular cartilage, Biophys J 101 (4) (2011) 916–24.
[38] M. D. Buschmann, A. J. Grodzinsky, A molecular model of proteoglycan-associated electrostatic forces in cartilage mechanics, J Biomech Eng 117 (2) (1995) 179–92.